
Article:
Lewinska, Paulina Barbara Wiktoria, Głowacki, Oskar, Moskalik, Mateusz et al. (1 more author) (2020) Evaluation of structure-from-motion for analysis of small-scale glacier dynamics. Measurement. pp. 1-15. ISSN 0263-2241

https://doi.org/10.1016/j.measurement.2020.108327

Evaluation of structure-from-motion for analysis of small-scale glacier dynamics

Paulina Lewińska[1,2]

Oskar Głowacki[3,4]

Mateusz Moskalik[3]

William A. P. Smith[2]

[1] AGH University of Science and Technology, Faculty of Mining Surveying and Environmental Engineering, al. Mickiewicza 30, 30-059 Krakow, Poland

[2] University of York, Department of Computer Science, York, UK

[3] Institute of Geophysics, Polish Academy of Sciences, Warsaw, Poland

[3,4] Marine Physical Laboratory, Scripps Institution of Oceanography, La Jolla, USA

Corresponding author: Paulina Lewińska, ORCID: 0000-0002-8141-754X, email: lewinska.paulina@gmail.com

ACKNOWLEDGEMENTS: The article was prepared under the research subvention of AGH University of Science and Technology No. 16.16.150.545 in 2020, Polish National Science Centre Grant Number: 2013/11/N/ST10/01729 and from the funds of the Leading National Research Centre (KNOW) received by the Centre for Polar Studies for the period 2014–2018.

Abstract

Measurement of the geometry of marine-terminating glaciers is challenging due to the lack of stable ground areas in close proximity to the glacier. This precludes the use of fixed measuring devices and restricts the placement of ground control points. We propose a measurement procedure for marine-terminating glaciers using structure-from-motion including proper survey planning, control point design and model alignment. As a case study, we surveyed Hans Glacier, Hornsund fjord, South Spitsbergen. We demonstrate that our method is indeed effective for documentation of small-scale glacier dynamics, show the importance of appropriate alignment strategies for models with poorly distributed control points and compare two SfM tools (Agisoft Metashape and Bentley ContextCapture) concluding that ContextCapture offers around 17% lower error, 25% faster processing and better reconstruction of fine details and shadowed concavities.

Keywords: structure-from-motion, GCP placement evaluation, Hans Glacier, glacier terminus dynamics monitoring

1. Introduction

Low equipment costs and the availability of fully automatic, reliable and accurate software tools has made structure-from-motion (SfM) widely-used in geomorphological studies [1–3]. Early work used SfM for documenting rock formations, bedrock ridges, hills and other small, static structures [1,4–6]. The utilization of unmanned aerial vehicles (UAVs) for data gathering allowed enlargement of the area of observation to farmlands, spoil tips, open-pit mines and quarries [7–9]. Other applications include the monitoring of dynamic environments such as landslides, riverbanks and seashores. All the above-mentioned geographical settings need accurate surveys in order to calculate changes in volume and material content. The motivation is the same for measurement of glaciers [10] and snow cover [11].

The accuracy of SfM methods is still debated [12–14]. In a measurement science setting, a very recent study quantitatively evaluated the accuracy of dense models obtained with SfM [15,16]. However, they used a contrived setup of a scale model of a river floodplain with ideal mounted camera positions. This allowed for almost unlimited ground control points (GCP) placement which is not feasible in many real word situations. Another recent study evaluated the effect of the number of GCPs in a large-scale UAV survey of static terrain [6]. Their goal was to choose the proper flight plan and acquisition method for this area while GCP analysis was a secondary aim of this study. While evaluations of SfM methods have grown in number over the past few years, only a small number of them describe in detail the problem of GCP placement and those that do usually involve UAV-based data acquisition. What is more, GCP placement studies often describe study areas where their placement is not limited to a large extent by safety measures or natural hazards. To our knowledge, none of the current studies undertook analysis of GCP placement in surveys done with hand-held cameras where data acquisition was performed from the level of the object. In order to fill in the gap in GCP placement analysis, a study was conducted on highly dynamic and remote object that is a water-terminating glacier. It allowed us to evaluate hand-held camera-based setups for SfM, their limitations concerning GCP placement restrictions and the effect that various types of GCP have on the accuracy of short term spatial monitoring of large natural. This is important since, due to the mobility of the survey setup for SfM, this extends the use to hazardous, remote areas, where other means of gathering dense 3D information are limited either by safety of the equipment or the people involved. However, this can be only done with a suitable GCP placement strategy, image acquisition strategy, model registration pipeline and the likely accuracy of the results can be predicted beforehand. This paper aims at the creation of such a method.

1.1. Contribution

In this paper, we consider a real world, highly challenging and practically important measurement scenario: modelling the small-scale dynamics of marine-terminating glaciers. This scenario is challenging because GCPs can only be placed on the very limited stable ground regions at the edges of the glacier (often only on one side) and uncertainty increases away from these areas. In addition, fixed camera positions cannot be used since the majority of the glacier is only visible from sea or air. Dynamic changes to the glacier terminus are practically important because they allow the occurrence,

frequency, and size of small- and large-scale calving events to be measured. However, the changes can be quite subtle and so high accuracy is required to resolve them. For a realistic representation of this scenario, we conducted nine SfM surveys of the Hans Glacier, a marine-terminating outlet glacier located on Hornsund fjord, South Spitsbergen. We seek to evaluate the suitability and performance of SfM in this setting. In so doing, we make a number of contributions.

First, we show that SfM algorithms applied to imagery collected from a handheld, uncalibrated camera can be used as a fast and accurate means of obtaining 3D information on a glacier front. Second, we evaluate how the placement, type and number of GCPs influences the geolocalisation of the model. Third, we distinguish different measures of accuracy and transformation strategies for aligning models. Fourth, we compare the accuracy of 3D glacier front models created using two different popular software packages, Agisoft Metascan (AM) [17] and Bentley's ContextCapture (CC) [18]. Finally, we discuss the significance of obtaining 3D data in relation to calving event monitoring and terminus position change.

2. Challenges in monitoring of glacier dynamics

2.1. Ice loss from marine-terminating glaciers

The annual ice loss from glaciers and ice sheets between 2003 and 2008 was estimated to be $1.51\times10^{-3} \pm 1.6\times10^{-4}$ m in sea-level equivalent [19]. This freshwater supply is not only responsible for a significant rise in global ocean levels, but also changes the thermohaline structure of polar seas, which impacts marine ecosystems. For example, the melting of the Greenland ice sheet created a cumulative freshwater anomaly of $3.2\times10^{12} \pm 3.58\times10^{11}$ m^3, which potentially affects large-scale Atlantic Meridional Overturning Circulation [20,21]. Marine-terminating glaciers and ice sheets are losing mass worldwide as a result of three major processes: (1) freshwater discharge, (2) submarine melting at the ice-ocean interface, and (3) iceberg fluxes from the glacier terminus [22]. The first of these is directly connected to surface melting, rainfall episodes and water circulation in subglacial conduits. Submarine melting rates depend, in turn, on water temperatures, which are now rising rapidly as a result of climate shifts [23]. The solid ice discharge, also known as, 'iceberg calving', can be defined as mechanical loss observed at the edges of ice shelves and glaciers [24]. It accounts for around 40% of the mass loss from the Greenland ice sheet [25,26]. However, accurate quantification of glacier velocity is usually required to calculate volumes of icebergs that break off from the ice cliff. Therefore, measurements of both temporal changes of glacier terminus positions and calving intensity are essential to understand small-scale glacier dynamics and their relationship with external driving forces, including heat exchange at the ice-ocean boundary. These details are needed for more accurate estimates and modelling of the contribution of marine-terminating glaciers to the eustatic sea level rise.

2.2. Measuring small-scale glacier dynamics

Glacier velocity is an important factor in glacier behaviour, but it is challenging to measure daily changes with a high spatial resolution. Satellite-based remote sensing methods are useful in the case of observing larger events or long term glacier front displacement [27,28]. The level of detail of small-scale calving events, represented by a raster on the cell (pixel) size, or spatial resolution of satellite images or aerial based digital elevation model (DEM) is not high enough for

such analysis. Another issue is the temporal resolution of the satellite; satellites with higher spatial resolution (e.g. Landsat-8) have longer periods of time between revisits. Taking into account clouds that can appear on the image, the number of data points is limited to a dozen or so usable images per year. This problem can be partly mitigated by using airplanes or UAVs [29,30]; however, these methods are still evolving. Time lapse photography can be more effective while observing calving events and their frequency [31,32], however, it usually does not allow for volume measurements since it rarely utilises stereo-images [33]. Novel approaches, like terrestrial laser scanning, are currently emerging [34–38], but this method is expensive due to the cost of the laser scanner and registration software. The laser scanner provides a 3D model of an object called a point cloud that can be geo-referenced with survey points of known coordinates [39]. Dense point clouds can be easily converted into a mesh model, allowing for volume calculations. Currently it is possible to buy a terrestrial laser scanner with a range of a few km and accuracy of a few mm that seems like a perfect solution for glacier observations. Due to the uniqueness of the laser beam being used, however, it is highly sensitive to weather conditions such as water vapour. Another way of surveying tidewater glaciers would be the use of SAR (Synthetic-Aperture Radar) sensors, since they are not susceptible to weather conditions. This method has its limitations since the time of revisit depending on the source could be from six to twenty-four days, that makes day-to-day measurement impossible. In addition, a pixel size of a few metres, makes this method useful for large glaciers with daily ice loss of at least a few metres, but might not be sufficient for smaller ones with more subtle variation [40].

2.3. Structure-from-motion in glaciology

SfM offers the potential of filling the gap between expensive, but accurate laser scanning and cheap but limited traditional survey and satellite imaging or time-lapse photography [41]. In addition, SfM requires only a conventional camera which is more portable and offers faster acquisition than a laser scanner. It is therefore applicable for measurement of marine terminating glaciers where much of the terminus may not be visible from a stable vantage point. One of the first uses of SfM was for monitoring of periglacial processes [29,42–44] of alpine or more general mountain glaciers. The results of those studies have shown the high flexibility of this method in terms of time management during field works and most importantly the amount of data that a relatively short survey can obtain. Combining SfM with UAV-based pictures and movies has enabled modelling of parts of glaciers and its surroundings with detail rarely seen before. SfM accuracy is often described as worse than those of laser scanning, however the range is usually much larger [13,42].

Studies of marine-terminating glaciers followed alpine glaciers monitoring [4] and the results were equally satisfactory with a large emphasis on the fact that the survey could be carried out from outside the structure, thus limiting the time and effort needed to move along the object. The most important problem that was observed was the placement and stability of ground control points– elements used for ensuring proper scale and/or georeferencing the model. For marine-terminating glaciers, this issue was important since it required placing points in close vicinity of the glacier or on its

surface. It was not always possible to place or measure them on or around the object [4,43] and therefore to give the models proper geolocalization or scale.

In the case of UAV acquisition this problem can be mitigated in two ways. Either by choosing a number of natural elements as GCP and measure their coordinates from a distance (single long-range laser scan, tachymetry, triangulation detailed DEM etc.) [29,42,45] or with the use of dual-frequency GPS receivers placed on the UAV [3]. The first approach is more versatile since the UAV does not need to have an extra GPS unit thus any UAV can be used for the survey. However, GCP might move over time, with each UAV survey there should be a control measurement of their coordinates [12]. This can be mitigated with the second approach, that can be done either by expensive off-shelf solutions [46] or custom built units with dual-frequency receivers on board, and GPS base station on the ground [30]. This approach is more suited for dangerous areas but can be done usually only with fixed-wing airframe UAV. Both of those can be adapted into ground-based SfM survey.

Midgley and Tonkin [47] show that SfM can be also used in order to create models out of archive data. The authors decided to use SfM software to create a 3D model of former shape, volume and placement of marine-terminating glaciers in Svalbard. For this purpose they obtained images taken in 1936 with an analogue camera, digitized them and applied SfM. Contemporary LIDAR data was used for geolocalisation of the resulting models. This example shows that, despite the fact that the accuracy of 1936 model might not be high by current standards, the overall results allowed for measurement of long-term changes to the glacier terminus.

All of the described research puts a lot of emphasis on two major issues. Firstly, the results were not always repeatable in regard to range, quality, number of artefacts and sometimes the shapes. Secondly, there was a general problem with placement of the control points – the number, type, survey method and most importantly the placement along or around the glacier. Since due to various field conditions, GCP cannot be eliminated entirely, even with experiments such as [30], analysis of their usage in regard to overall results of the survey needs to be performed [48].

3. Methods

3.1. Structure-from-motion software

Strictly speaking, SfM algorithms seek to estimate 3D scene models (sparse point clouds), camera intrinsic parameters (focal length, centre of projection etc) and camera extrinsic parameters (3D pose – i.e. a rotation and translation) from a set of overlapping images. Sometimes it is assumed that the cameras are calibrated, i.e. that intrinsic parameters are already known. In general, SfM algorithms proceed by first extracting a set of distinctive local features in the images, robustly matching them between images, optimising the 3D position of these matched features and the camera parameters and iteratively adding more images to the reconstruction. The outputs of this process are the camera parameters and a sparse point cloud with one 3D point for each matched 2D feature [49]. Subsequently, with the camera parameters fixed, a dense point cloud can be estimated using a process called Multi-View Stereo (MVS). Often this is based on performing

dense binocular stereo between pairs of images with large overlap and then combining the multiple depth maps. Sometimes this dense point cloud is transformed into a surface by fitting a triangle mesh and the point cloud or mesh may be scaled and georeferenced using GCPs [50–52]. We refer to this whole pipeline as SfM and it may be implemented in a variety of different ways [53–55].

For this study, two SfM software packages were used: Agisoft Metashape (AM) and Bentley's ContextCapture (CC). These are closed source, commercial packages for which the producers do not disclose implementation details. Nevertheless, they are very widely used, including in the glaciological community. AM appears to follow the pipeline sketched above and works better with images taken in a fashion similar to stereo image photo acquisition. The workflow of CC suggests that it is not based directly on stereo images but since such image configurations can be successful for both CC and AM it was decided to take images in this fashion. In order to add scale to the object or to provide geo-reference, control points, elements of known dimensions or coordinates are used.

3.2. Control point placement strategy and photogrammetric survey.

We used nine series of photographs of Hans Glacier, a marine-terminating outlet glacier located on Hornsund fjord, South Spitsbergen. This glacier is about 1,30 m wide [47], and its front velocity has been estimated at 200 m/yr and front retreat at about 40 m/yr [26]. For our survey, four types of control point were used. In order to facilitate the commonly used approach in photogrammetry we placed artificial GCPs on a rocky beach that ends near the West part of the glacier terminus (Fig. 1). They were designed as black and white checkerboards of exactly 0.20 m × 0.20 m (each black or white square was 0.10 m × 0.10 m) with black and white (0.01 m × 0.02 m) rectangular panels on each side. Their number and placement was significantly limited by tidewater covering large parts of the beach. However, their dispersion is enough to fulfil the requirements of geometry of control point placement during the survey. Control points were measured via GNSS unit in a stop-and-go fashion using Polish Polar Station Horsund GPS base. The GPS measurements were carried out with the GNSS (Global Navigation Satellite System) receiver that was set up for the scientific crew of the Polish Polar Station and was available for us to use. It was set up at the time to only receive GPS signals. The exact size of the GCP allowed the coordinates of the middle (the place where all four smaller squares met) to be obtained with an accuracy of 0.04 m for XY and 0.07 m for Z.

In order to add extra control points to the three artificial ones a second set of GCP was chosen. These were natural control points on the same beach and consisted of rocks that were large enough not to be moved by the tide. This allowed for better dispersion of control points in relation to the glacier. The accuracy of GPS measurement was similar, however, since these elements do not have such a well-defined central reference point like the artificial control points have, they are less likely to be pinpointed on the images with the same accuracy. Thus, it was estimated that their accuracy would be twice as bad as for the artificial GCPs, putting them at 0.1 m.

The third group of control points were designed on the 'dead' unchanging part of the glacier and on the rock near the glacier where the survey crew did not have access. This allowed for better dispersion of the GCPs than the other groups since some of them were placed on the object itself and on wider range of heights, giving better geometric constraints. The unchanged areas were pinpointed from the time-lapse images taken with a GoPro 3 black camera (resolution 12.1 MP, pixel pitch 1.55×10^{-6} m, focal length 2.92×10^{-3} m). There, a set of six unchanged, clearly indefinable elements was chosen. Their coordinates were taken from the first geolocalised model (11 August 2016) and their accuracy was derived from the accuracy of this model with a small factor added due to potential problems with identifying the same point on all the models, putting the accuracy at 0.15 m.

Additionally, five stable points on rocks were measured with a GPS unit to be used as control points (CP) for accuracy evaluation. Their error was the same as with natural GCP, namely 0.10 m. Also, their coordinates were read from the base model (11 August 2016) with an accuracy of 0.15 m.

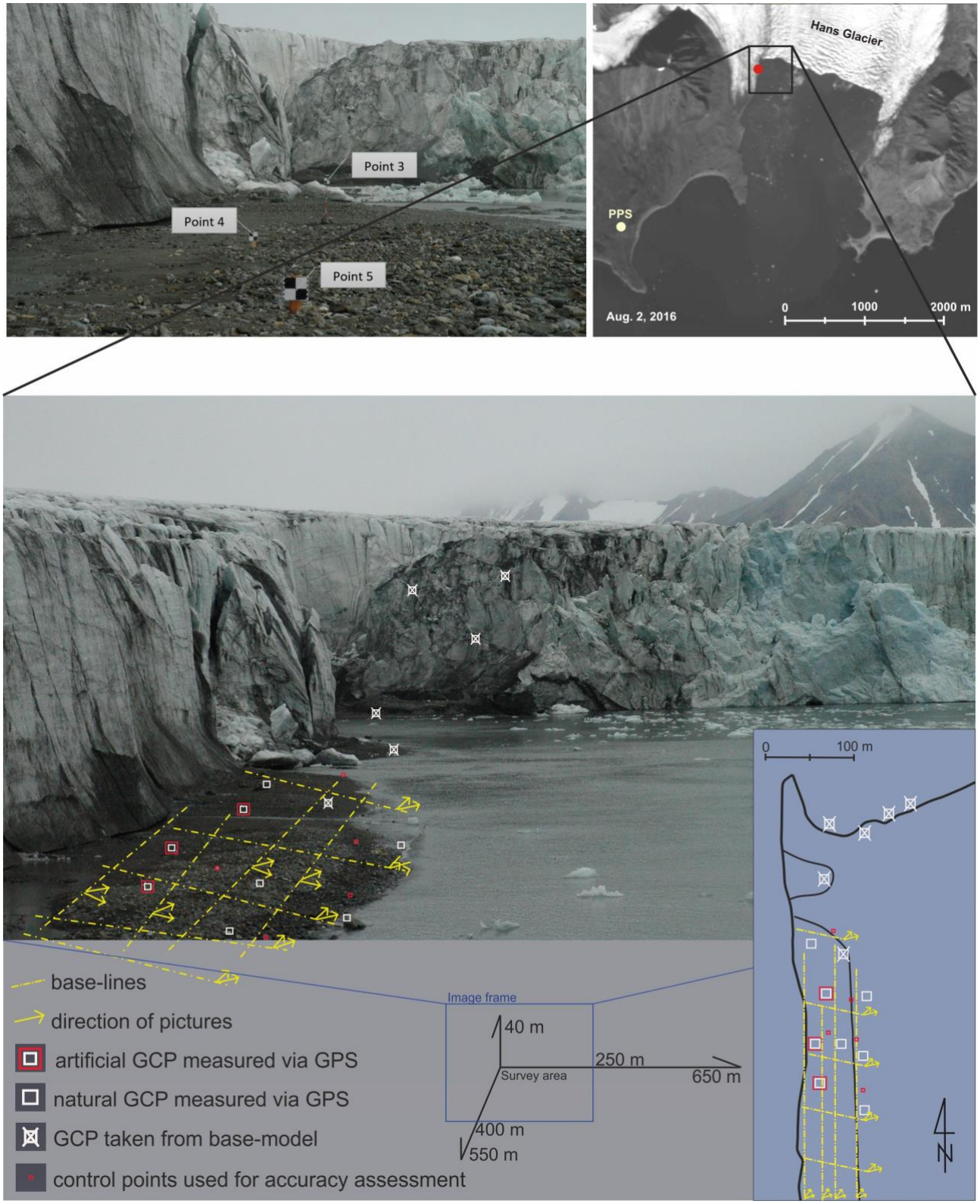

Fig. 1. Placement of control points on the beach in front of active part of Hans Glacier. The lower picture represents 1/3 of Hans Glacier area analysed in this study. PPS – Polish Polar Station.

Photo sessions were done while moving along base-lines located nearly parallel and perpendicular to the glacier front, on the same beach that markers were placed on. They were taken while aiming the optical axis parallel to each other and covered the glacier from the waterline to glacier surface. CC needs minimum three images to perform a 3D model, it was assumed that four sets of images would be a safe minimum – if any needed to be removed for quality or other reasons.

The minimum and maximum distance to the glacier front was 150 m and 1,100 m, respectively. The length of the beach was about 400 m and ended about 100 m before the glacier front. Each photo session consisted of at least three baselines with two sessions within them. The number of baselines were highly dependent on weather conditions and time management. The first baseline was always placed at least 70 meters from the control point located farthest from the glacier. The first set of images was done with the camera optical axis perpendicular to the glacier front. The control points were visible on at least half of those photographs. Another set was captured aiming at as large an angle as possible while still having control points within frames if possible. The first session aimed to ensure the appropriate number of photographs with control points, but did not provide large parts of the glacier front. The next were done in order to gather more geometrical information on the glacier front. The final base-line was done in between the first and last two markers or, if the water level was low, in front of it. Images taken closer and at an angle allowed for better coverage of fractures in the ice front, giving more details on their depth. The overall idea was to take as many images, covering as much of the glacier as possible, while at least 20% of the photographs should cover control points. The baselines and control points can be seen in Fig. 1.

The survey was done between 10 August 2016 and 22 August 2016. The number of obtained images is shown in Tab. 1 and ranges between 164 and 792 per session. We used a Nikon D70 with Nikkor AF-S lens (6.1 MP resolution, pixel pitch 7.78×10^{-6} m, focal length 1.80×10^{-2} m - 7.00×10^{-2} m). While more modern sensors offer higher resolution, the large pixel size and robust optics in this camera provide high quality images that work well in practice for SfM surveys. It is also representative of the sort of camera that might be readily available for use in such surveys in challenging environments.

4. Model construction and transformation

Registering each model to a common coordinate frame amounts to estimating a scale, rotation and translation. Where the common coordinate frame is a world coordinate system, this process is referred to as geolocalisation. AM and CC provide the residual error of this procedure. It is based on the distance between point coordinates on models after the transformation has been applied and comparing them with given XYZ coordinates of control points. This procedure, although mathematically correct, does not give the full picture of the error between model and world since it does not take into account control point dispersion, relation of the number of control points to the model size etc.

To assess the accuracy of the scale of the models and the geo-referencing procedure, models are compared against the XYZ position of control points and known distances between selected elements from GPS [56] measurements. For the purpose of this article, we define:

- *nominal accuracy* (accuracy of transformation as reported by the software),
- *real accuracy* (accuracy of geo-referenced models, calculated as the average distance between stable, unchangeable-with-time points from the model and GPS measurements - see Fig.1).

238 We divide the transformation pipeline into three stages:

239 • Geolocalisation with minimal control points - with the use of three control points (minimum required number).

240 • Dense model-to-model alignment – one of the point clouds/models was used as a base with extra control point
241 coordinates taken from this model, thus allowing for better dispersion of control points. This doesn't necessarily
242 improve the accuracy of geolocalisation but significantly improves the relative alignment between models.

243 • Geolocalisation best case – added extra control points from GPS measurements of natural elements (rocks) in
244 the glacier vicinity. Control point dispersion is still limited but this represents a realistic best case for our scene.

245 Accuracies of each type of GCP were used during each step of this experiment as weights and as such were added during
246 transformation within AM and CC software.

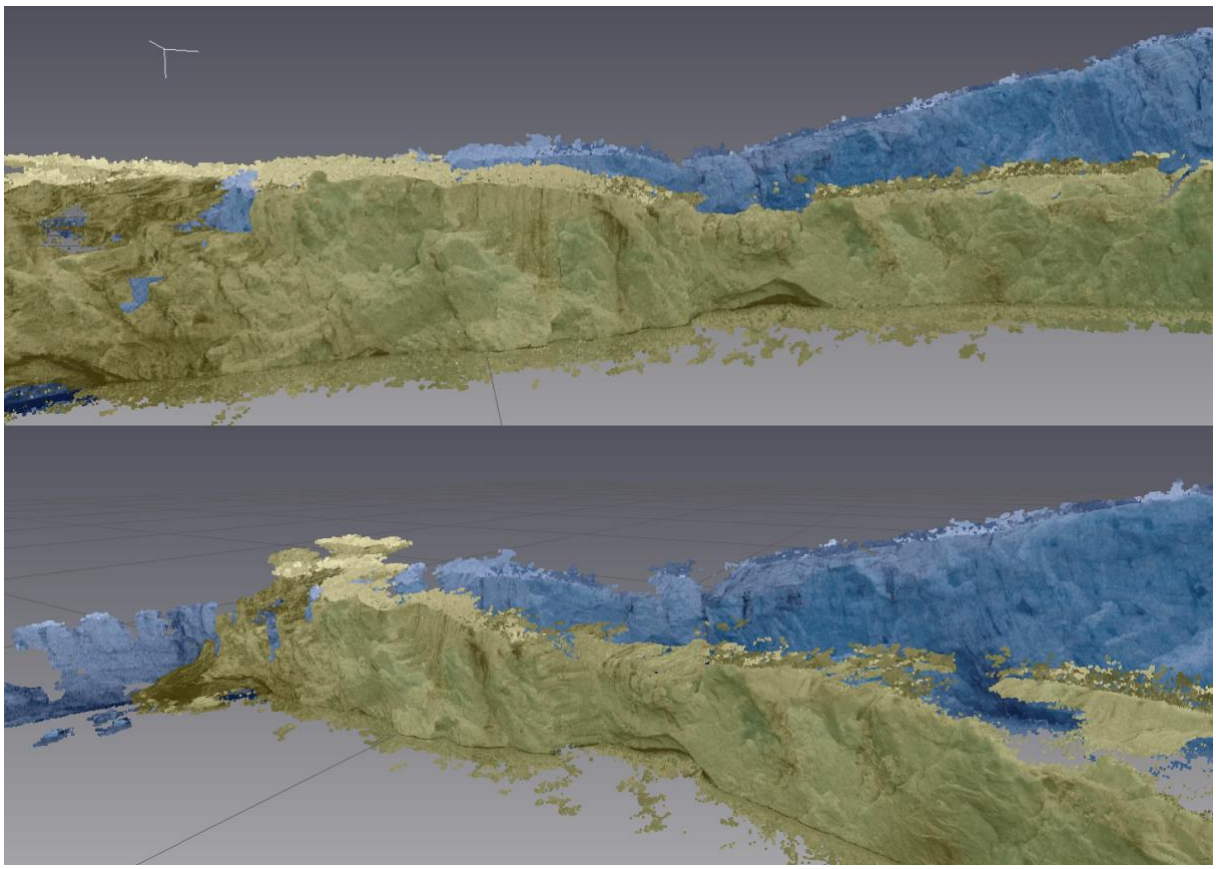

247

248 Fig. 2. Results of primary image-to-scene transformation process done in Agisoft. Blue - reference model (11 August
249 2016), yellow slightly tilted (16 August 2016) model.

250 **4.1. Geolocalisation with minimal control points**

251 Initial geolocalisation was done using three artificial control points placed in front of Hans Glacier. The nominal accuracy
252 of the AM 11.08.16 models was 0.11 m. Other data sets were primarily calibrated the same way and the nominal accuracy
253 is given in Tab. 1. While this error was apparently low, the result did not correspond well with the 'real' placement of the
254 glaciers. Some of the fronts were rotated vertically up to 28º, and two models were rotated both vertically and horizontally,
255 but to a much smaller degree up to 16º. This last issue was most visible in 20 August 2016 model (Fig. 2). 3D modelling

results did not allow for proper analysis of glacier front. Real accuracy was calculated based on five GPS measured control points, the error was from 0.5 m for points closest to the artificial control points and grew up to 5 m for furthest points, for all models besides 11.08.16. For this model, maximum and minimum error was 0.20 m and 0.61 m, respectively.

The results given by CC were noticeably different from AM outputs. All fronts were calibrated with average nominal accuracy of 0.41 m. None of the 3D models were rotated or moved to a large extent, less than 2°. In terms of real accuracy, the maximum error was 0.57 m for the furthest points and 0.20 m for points closer to artificial control points.

When comparing AM and CC models, they were significantly rotated and tilted relative to each other. The results suggested that although the nominal accuracy is good, it does not describe the real placement of the glacier. Additional adjustment was necessary in order to remove rotation.

		Geolocalisation with minimal control points			Dense model-to-model alignment			Geolocalisation best case		
Agisoft Metashape										
Date	Number of used photographs	Number of photographs with control points	Number of control points	Accuracy of adjustment (m)	Number of photographs with control points	Accuracy of adjustment (m)	Number of control points	Number of photographs with control points	Accuracy of adjustment (m)	Number of control points
10.08.16	660	-	-	-	308	0.323	3(0+3)	-	-	-
11.08.16	368	40	3	0.113	40	-	-	67	0.401	5(3+2)
12.08.16 morning	763	174	3	0.009	223	0.211	4 (3+1)	199	0.201	5(3+2)
12.08.16 afternoon	301	62	3	0.058	144	0.244	6 (3+3)	95	0.080	5(3+2)
13.08.16	233	32	2	-	102	0.107	5(2+3)	75	0.284	5(3+2)
15.08.16	244	59	3	0.072	84	0.321	5(3+2)	100	0.289	4(3+1)
16.08.16	792	180	3	0.530	242	0.241	6(3+3)	222	0.269	4(3+1)
20.08.16	179	56	-	-	99	0.109	4(0+4)	-	-	-
22.08.16	233	62	-	-	121	0.249	3(0+3)	-	-	-
ContextCapture										
10.08.16	541	-	-	-	228	0.344	3(0+3)	-	-	-
11.08.16	164	40	3	0.200	40	-	-	47	0.069	5(3+2)
12.08.16 morning	593	174	3	0.304	223	0.238	5 (3+2)	201	0.102	5(3+2)
12.08.16 afternoon	299	62	3	0.178	144	0.244	4 (3+1)	89	0.112	5(3+2)
13.08.16	233	32	2	-	102	0.310	5(2+3)	44	0.190	5(3+2)
15.08.16	244	59	3	0.113	84	0.189	5(3+2)	79	0.220	4(3+1)
16.08.16	632	180	3	0.499	222	0.321	5(3+2)	192	0.278	4(3+1)
20.08.16	166	56	-	-	90	0.281	4(0+4)	-	-	-

22.08.16	201	62	-	-	111	0.374	3(0+3)	-	-	-

Tab. 1. The number of used photographs of the glaciers front, number of used control points (in brackets number of placed control points + number of natural control points), nominal accuracy given by Agisoft and ContextCapture.

4.2. Dense model-to-model alignment

Dense model-to-model alignment of AM models was based on six additional points from the base model, unaffected by weather and the changing environment (top of boulders close to the glacier front, dead part of the glacier). Adding these points and, in the case of two last models (20 August 2016, 22 August 2016), eliminating previous control points improved the nominal accuracy. Not all base-model GCPs were used on all calculated models because points were not always visible on models from all dates or on sufficient number of images. The number and type of points used is given in Tab. 1.

Analysis of the AM point clouds shows improvement in the geographical placement of the glacier terminus position. The real accuracy was calculated using five stable control points (not used before), resulting in an average difference in XYZ coordinates of 0.36 m (not exceeding 0.57 m). Scale process was done correctly with an average accuracy of 0.18 m, with a maximum of 0.39 m.

Model-to-model alignment of CC models was done based on the same points as for AM. For the models calibrated before extra points did not change significantly nominal accuracy (Tab. 1) however they improved real accuracy. The average real accuracy of all models was 0.31 m, but with the maximum at 0.38 m. Scale estimation was done with an average accuracy of 0.21 m, with a maximum of 0.35 m.

4.3. Geolocalisation best case

Geolocalisation using a realistic best-case set of GCPs was based on five extra GPS points. As for model-to-model alignment, they could not be used on all models since at times recognition was indecisive (Tab.1). For the AM average, nominal accuracy was worst with model-to-model alignment, real accuracy was slightly better and the average was 0.35 m (not exceeding 0.60 m). Scale error was at 0.21 m, with the maximum at 0.41 m. For the CC nominal error, the transformation had not changed significantly and real accuracy was improved achieving an average of 0.29 m (not exceeding 0.38 m). Scale error was at 0.19 m, with max at 0.31 m.

5. Comparison of the mapping quality

5.1. Model comparison: resolution, range and artefacts

In order to compare models, reconstructions were performed in AM and CC using various settings so as to create similar point cloud density, similar mesh models (with similar density) and visually qualitatively similar, i.e. similar texture quality. This process has proven to be difficult due to different results with seemingly similar settings. Overall, CC generates a denser point cloud and mesh model than AM when using similar settings. The final results presented used

295 "medium" settings for AM and "normal" for CC. The resulting point cloud density was at 0.17 m for AM and 0.11 m for
296 CC. This also proves appropriate in relation to projected pixel size (i.e. the real world distance that projects to a single
297 pixel). The average pixel size for a single image varied from 0.07 m (closest to the baseline) to 0.38 m (furthest). CC has
298 significantly less texture options, however the colour and quality of the texture was qualitatively more realistic. Models
299 from each date differ in coverage, ranging from 1,000 to 2,000 m of glacier front. There were no distinct differences in
300 regard to range in CC and AM software. In each 3D model, artefacts were present which are now discussed.

301 For models constructed using AM, almost all of the glacier surfaces needed to be inspected and artificial elements
302 manually removed before further processing. There were small (up to 2 m) artificial elements placed mostly on the top
303 of the glacier or in its surroundings. Also, the glaciers top did not have a distinct edge – i.e. what should have been a
304 sharp boundary was overly smoothed in the reconstruction. This was less visible in the point cloud and more in the mesh
305 model. Calculating the mesh model with interpolation/extrapolation disabled improved the results, but still some parts
306 needed to be removed manually.

307 One of the most significant issues with AM models was that it did not correctly distinguish water reflection from the
308 glacier terminus calculating a 3D partial image of the glacier based on its reflection. This is a highly challenging scenario
309 for SfM methods based on feature matching. This occurred in four models, when the survey was done during clear sky
310 and glacier water reflection was significant. The 3D models constructed using ContextCapture had little to no artefacts
311 near the glacier terminus. Those were mostly ice reflections visualised as actual physical elements (Fig. 3). In AM, all
312 artefacts occurring in any stage of the calculation can be manually removed by the user, while CC models need to be
313 exported and another software tools used to remove unnecessary elements. However, with the limited number of artefacts
314 in CC models this was not a significant issue.

315

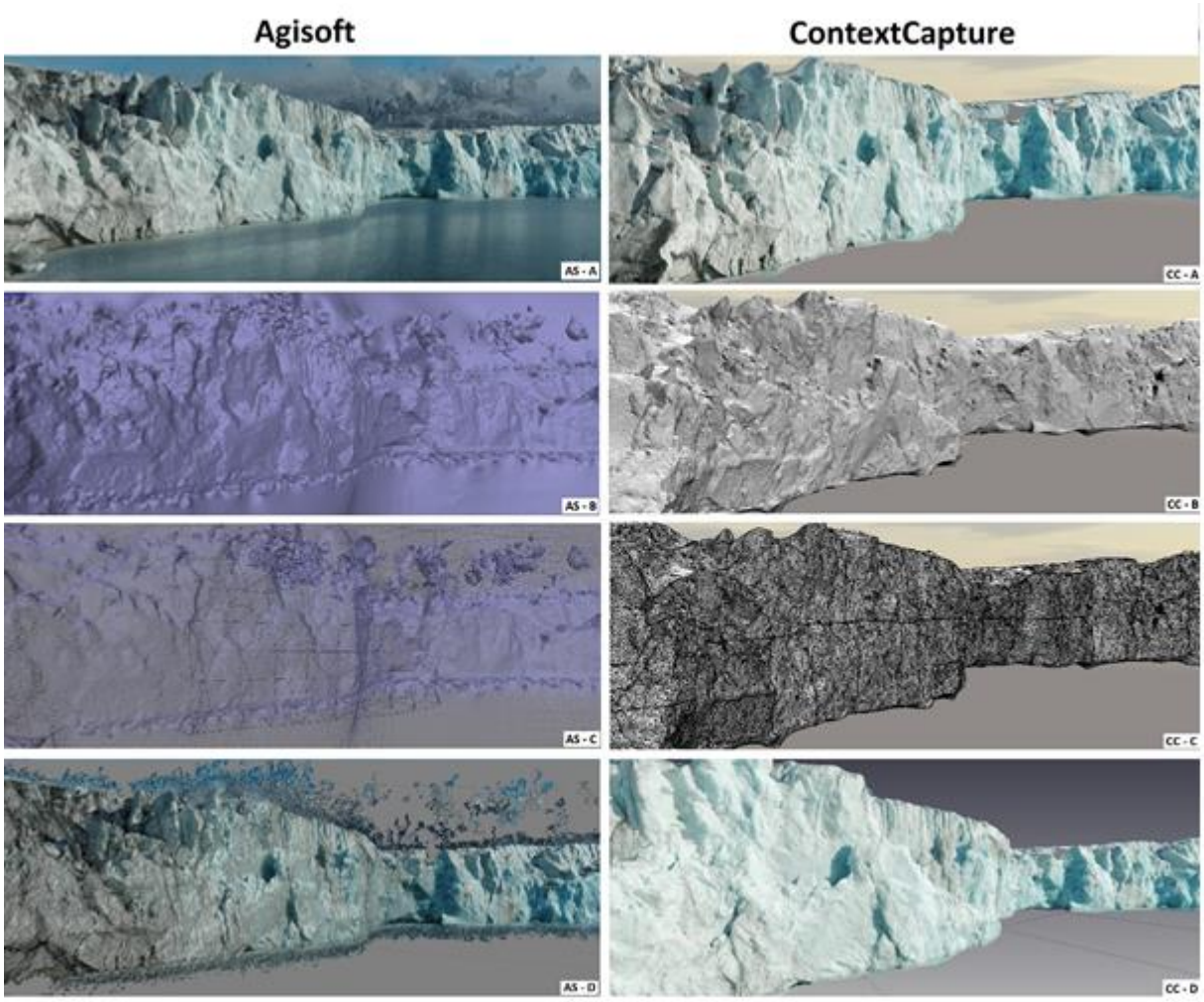

Fig. 3. From the top, textured mesh, mesh, mesh – triangles, point cloud.

5.2. Level of detail - modelling of voids

The level of detail in the models and, in particular, the *correctness* of void (i.e. concavities) depth and size are difficult [57,58]. The CC models are significantly more detailed as to their shape, size and more importantly depth of the voids. Voids are visible and their rough edges well-defined. In addition, when comparing the textured model and point clouds (or uncoloured mesh) it is apparent that the edges and discontinuities in the 3D model correctly align with the corresponding edge in the texture.

In the case of AM, most glacier terminus voids were interpolated with a false mesh placed at various depths or covering the crack completely. Also, there are many falsely calculated points in the point cloud that fill the cracks. Edges are almost completely missing. Each void is smaller and shallower than in CC models and also the edge placement does not correspond with the texture – usually the crack is smaller than the texture shows. This problem can be only partly mitigated by creating the mesh without interpolation/extrapolation. For large scale objects the mesh is more defined and sharp, but still not as detailed as in CC. Smaller voids are either filled or have no mesh at all. This results in a false area change and false volume change between calving events.

6. Application of SfM in the analysis of small-scale glacier dynamics

6.1. Calving analysis

Calving is described as a process of ice mass loss from the glacier terminus that is responsible for most water from land transfer [24,59]. Calving as a process can differ in accordance with the geographical placement of the glacier, frequency, styles, magnitudes, volume etc. Some of those aspects can be measured and analysed via satellite images [60–62]. But ground-based time-lapse photogrammetry brings more detailed information, especially in description of calving style [32,61,63]. 3D models can only improve this, especially if they were to be done in a time-lapse manner ergo, creation of succeeding 3D models in minor step [64].

A cross section of the Hans glacier models was studied (Fig. 4,5 and 6), representing the part of the terminus that undergoes most frequent calving during the survey period. 3D representation allows us to observe the mechanics of each event. In this example, the first event occurring between 12.08.16 and 13.08.16, led to loss of ice material, larger in the top part of the terminus and smaller in the bottom part. In between 13.08.16-15.08.16, the glacier moved forward, visible in the bottom part of the terminus, but it also bends from the top part to the front. In between 15.08.16 and 22.08.16, a larger event occurred covering a large slab of ice oriented almost perpendicular to the water surface. Models from between 15.08.16 and 22.08.16 that are also available and show no large calving, were omitted from the figure for better representation. This cross section shows the middle part of the glacier terminus. The events had common scenario and could be described as large in regard to the volume. Calving events in other parts of the glacier were also documented and their scenario differs.

Similar geometry analysis can be done for other voids and glaciar gates (openings that allow for the meltwather flows to exit the glacier) of the glaciers front. One of the examples can be seen in Fig. 4. Where it is visible that over time the gate changed its shape, size and placement. It started as a characteristic gate structure. Between 12.08.16 and 13.08.16 a calving occurred almost destroying the structure. Between 13.08.16 and 15.08.16 glacier moved forward changing the shape of the void and between 15.08.16 and 22.08.16 ice material loosen creating a new gate a few meters to the right of the original structure. Between each date occurs a void representing the amount of material being detached from the main body. It is possible to measure the distance between the terminus before and after calving and, by isolating the calved area, to perform volume calculations. During calculation, it is necessary to take into consideration the terminus movement described above. This number might be negligible for larger sequential events not producing a large error in volume calculation but for smaller events, it needs to be factored in. The models provide a probable assumption of the terminus movement that could be included in calving volume calculation.

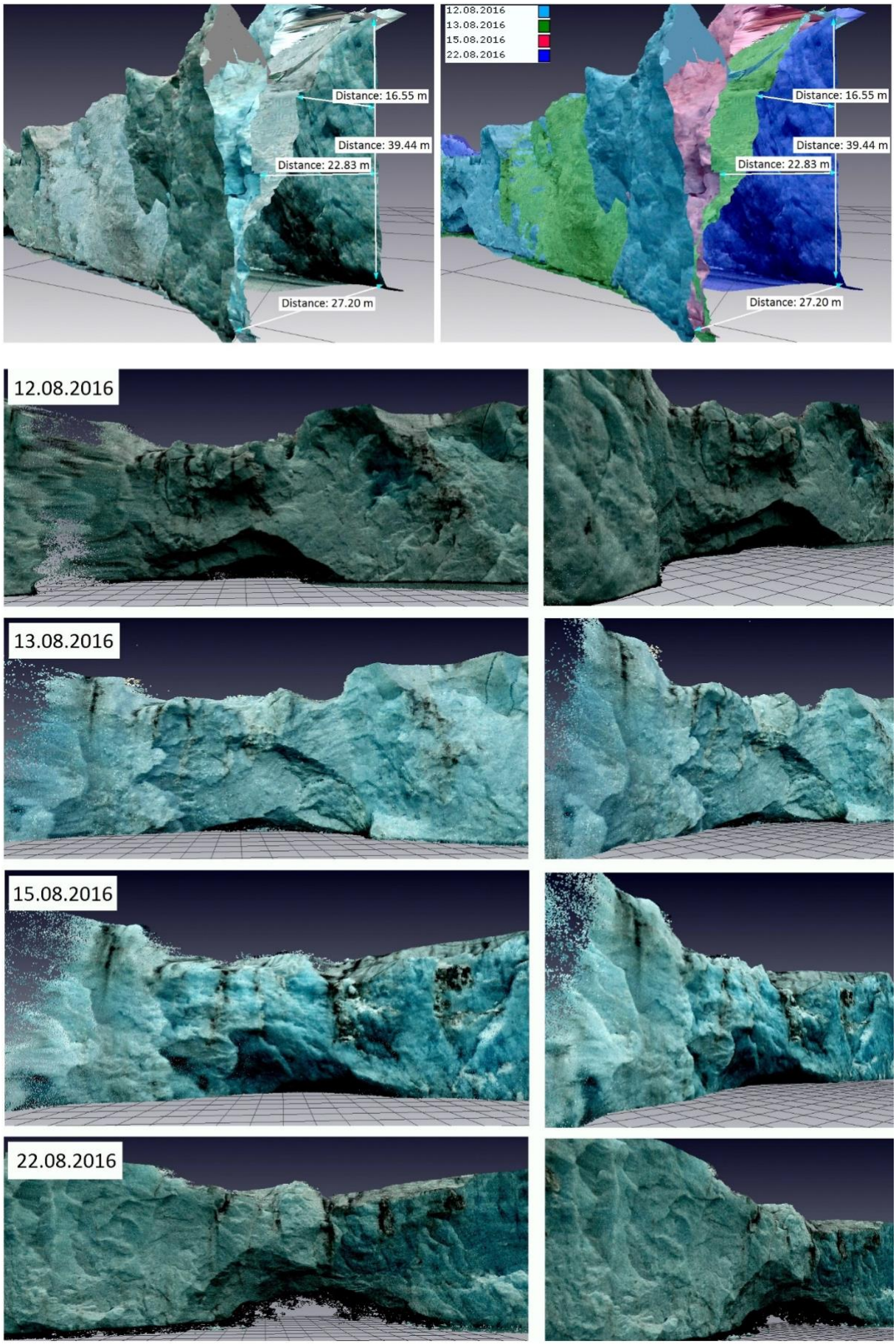

Fig. 4. Top: Cross-section of Hans Glacier showing the void created during calving events. Bottom: Glacier ice gate evolution.

366 **6.2. Terminus dynamics monitoring**

367 Glacier velocity is measured often nowadays. Long-term observations can be done successfully with the use of satellite-
368 based data [65,66] or aerial images [66,67]. But, this is limited by the availability of satellite data and atmospheric
369 conditions in the case of planes and UAV [68]. Terrestrial images have been taken [69] in order to allow to monitor
370 terminus dynamics thus proving that this is a useful method of data collection. Time-lapse cameras that can be installed
371 in remote areas have shown to be useful for smaller glaciers or more detailed analysis [70,71]. They allow movement
372 trends in different regions of the glacier terminus to be distinguished [10,71,72]. Various organizations have installed
373 time-lapse cameras to monitor glacier termini in various parts of the world. The British Geological Survey installed
374 cameras monitoring Iceland's glaciers [73,74], the Extreme Ice Survey has cameras in Greenland [75,76] and the Polish
375 Polar Station Hornsund has cameras placed around Hans Glacier. However, this usually provides 2D data and, as has
376 been observed, 3D models of the glacier front give more insight into the mechanisms of its movement.

377 In the case of the Hans Glacier, GPS survey of stakes placed on the surface were being done every two weeks until 2018.
378 Also, additional GPS survey (during summer) was performed in various time periods [77]. The survey (5_{th} and 24_{th} of
379 August, [78]) show terminus velocities from 87.60 to 2,190 m/yr, with an average of 146-182.5 m/yr. Those results are
380 based on measurements of one or two GPS stations placed close to the glacier front. The real accuracy of point clouds
381 described in previous sections was at around 0.30 m. This accuracy does not allow daily analysis of glacier position since
382 estimated daily movement is less than 0.30 m. However, it is possible to see the pattern of movement that can be used in
383 more long-term (weekly or monthly) analysis.

384

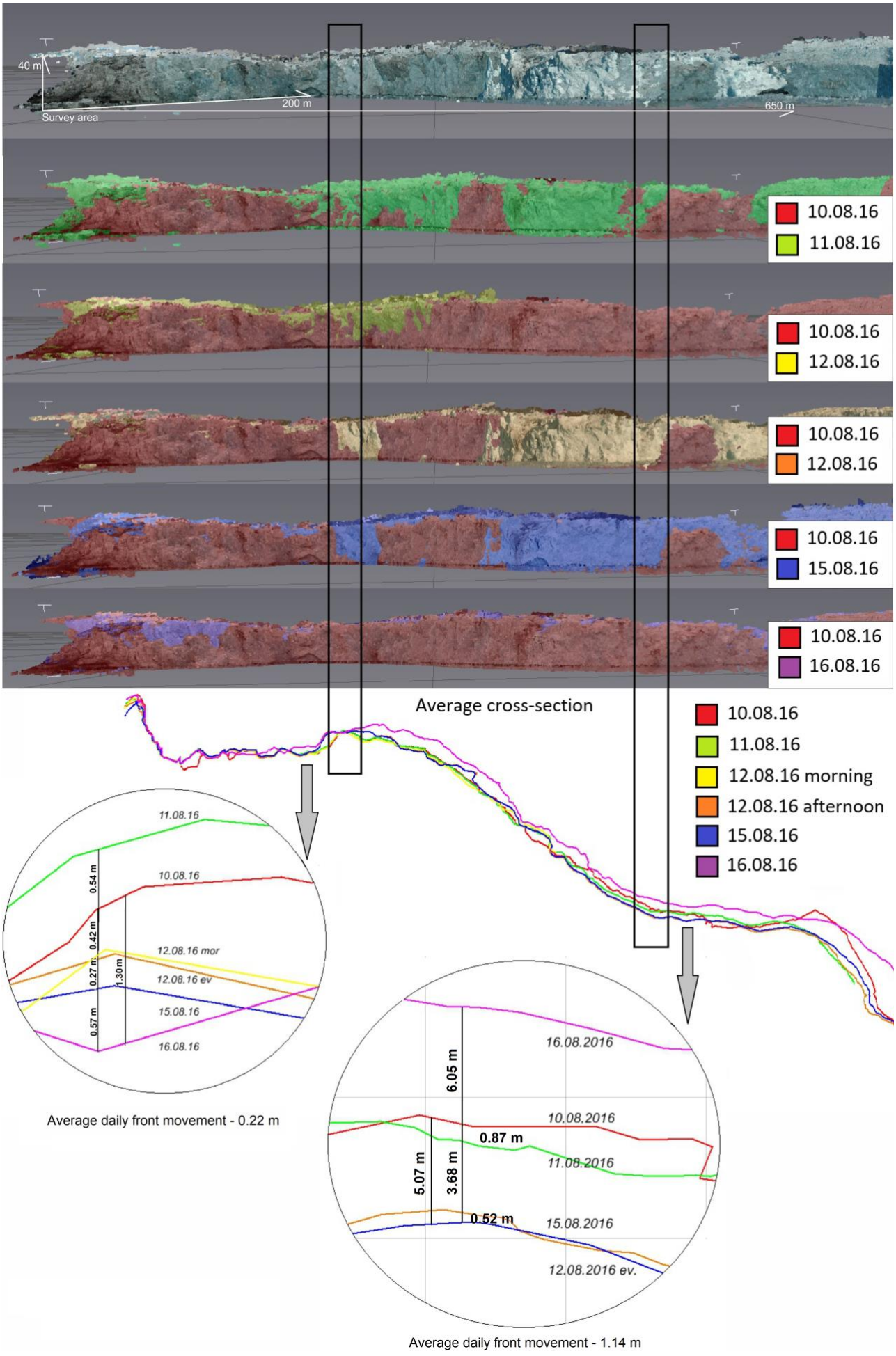

Fig. 5. Calculation of the glacier front movement.

Movement calculation of the Hans glacier terminus was done with the use of point clouds obtained after model-to-model transformation based on a 650 m long segment of the glacier terminus visible in all CC and AM point clouds. Measurements were collected on sections of the glacier front that did not undergo calving. Areas, for this part of analysis, were isolated with the use of two indicators, first, time lapse photography done every second during the SfM photo survey, second, finding areas with largest differences in volume occurring between each photo survey, done with the use of CloudCompare software [79]. Average daily glacier front speed was at about 0.47 m, but results differ significantly between days (Fig. 5). This result corresponds well with previous assessments. After the differences in front position are calculated, calving areas are easily located and analysed. Events can be isolated from the front and 3D model differences before and after each calving event compared to give the overall volume of ice loss.

Figure 6 shows an example of the analysis of the entire modelled front. It is possible to analyse and visualise in detail both carving events and glacier front movement, measure there volume and current front placement. What is more basing on the cross sections a detailed analysis of the mechanics of ice mass movement is possible, providing necessary data for not jet fully understood processes of glacier advance and retreat mechanics.

Hans Glacier, front movement is relatively small (73-110 m/yr). However, in the case of Greenland glaciers, larger ice shelf terminating glacier velocities can range from 300–1670 m/yr, and the average marine terminating glacier velocity is 1,890 m/yr [80]. Therefore, the daily movement at large Greenland glaciers is more than 1.00 m, and an accuracy of 0.30 m are within the acceptable range. If the necessity of monitoring glacier termini with daily movement around or below 0.30 m would occur, it could be done with the use of cameras with greater resolution and, if possible, with the use of better suited points, taking into account the limitations of the method previously described (control point placement, transformation procedure, etc).

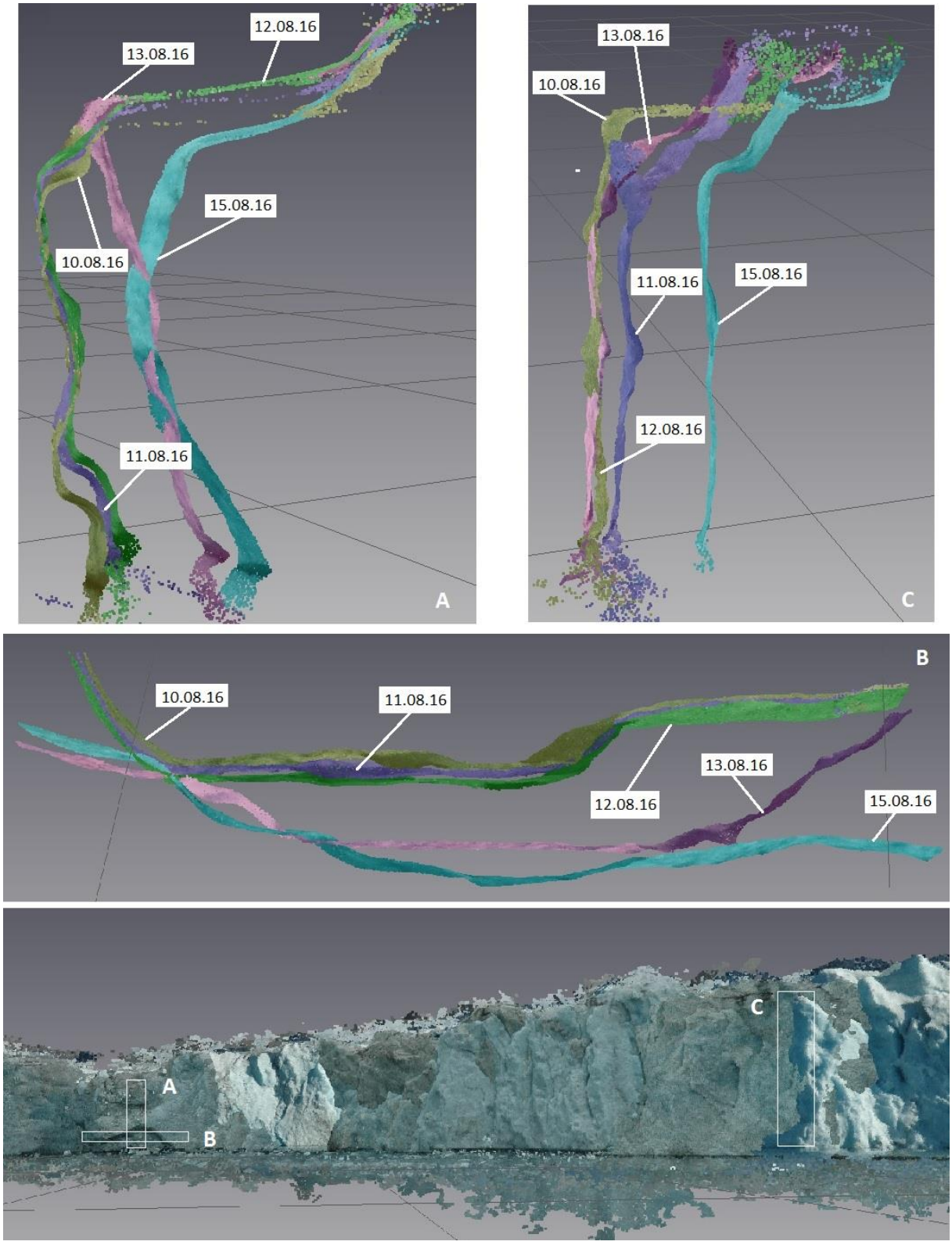

Fig. 6. Bottom – view of 3D models of Hans Glacier. Top – cross-sections thru point clouds showing front movements (C) and calving (A and B). Results from Context Capture.

7. Discussion and Conclusions

The main aim of this study was to propose a method of performing a 3D inventory of glaciers in a way that would allow for accurate small-scale movement observations, and to analyse various GCP configurations in order to make this process

as accurate as possible. We estimated that, with limited access to the glacier, two methods of GCP placement are most reliable.

The first method involves placing a small number of GCPs in front of the glacier terminus, creation of a base model with SfM and limited GCP and using this model as a base for obtaining GCPs for other models. This method has proven to be the fastest during each data set acquisition, since the user needs to place only a limited number of GCPs on the images and the GCPs need to be measured just once and can be placed further from the terminus on a safe part of the land. In addition, it is the easiest to process since the user can choose GCPs from the much larger span of the complete modelled area. The only drawback of this method is that limited number of physical GCPs does not place the base model exactly in the chosen global coordinate system. However, this is of limited importance if only day-to-day changes are being observed. The second method involves a larger number of GCPs some of which are well-defined (e.g. purpose-built checkerboards) and some natural. This method is significantly more time consuming during the data acquisition since the changing water level often destroys or covers natural control points and moves the well-defined GCP. This means they need to be measured during every survey session, prolonging the time of the survey. Also, the user needs to label them on the images. During processing, natural GCPs are usually hard to distinguish and unambiguous identification is difficult. This all prolongs the time of processing, leading to many iterations of this process in order to get satisfactory results. In addition, with almost-planar GCP placement (as occurs when distributing them over a beach) on only one side of the modelled object it is not certain if each model will have enough GCPs to be accurately placed on global coordinate system until processing is complete. Considering all this we propose the first method for day-to-day analysis or seasonal observations and second method for long term or less frequent observations.

The demand for 3D models is increasing as more emphasis is given to proper description of Earth-forming processes, and glacier front change is one of them. The SfM methods provide a straightforward and accessible means of constructing a 3D glacier model. Multiple models can then be used to visualize the calving process and general front movement [27,78,81]. Additionally, mass loss, stages of calving, and/or glacier gate creation can be monitored, described, and, as a result, understood. It is possible to tie them to other spatial data, weather conditions, tides etc.

Our main aim was to show how SfM can be used to create accurate models of glacier fronts with the use of images from a hand held camera and how those models can be used for detailed analysis of front movement and calving mechanics. In doing so, we arrive at a number of key conclusions:

- Different SfM software tools can give quite different outputs. Glaciologists and Earth Scientists need to be aware of this and understand how to validate their reconstructed models.
- Nominal accuracy, as reported by SfM software, is not reliable in terms of the geographical placement of a model; they can only be used to assess scale estimation.
- SfM models need to be validated by other independent survey (GPS, laser scan etc.)

445 - Using the theoretical minimum number of GCPs placed on one side of a glacier are not enough for proper image-
446 to-scene transformation. This can produce significantly rotated models out of the ground plane.
447 - In terms of accuracy of the scale and geolocation of a model, it is better to have larger number of less-defined
448 control points (rocks) than a smaller number of well-defined points (checkerboards).
449 - AM based models need more and better-dispersed GCP to achieve correct scale and placement than CC based
450 models.

451 In addition to these general conclusions, comparison of workflow and performance of two SfM software packages was
452 done. While performing calculations using similar settings, the speed of each step of the pipeline was in favour of CC by
453 about 25%. In CC, the georeferencing process could only be done before other calculations. If an error in this procedure
454 occurred, it was visible only after the point cloud was produced. An error might be mitigated only by adding/editing
455 control points and redoing all calculations. That prolongs the process significantly. With AM GCP can be added at any
456 time, thus allowing for multiple versions of GCP placement to be analysed fast and any mistakes in GCP coordinates or
457 placement fixed. Also, in contrast to CC, workflow in AM, allows for control points to be placed into a model and then
458 their placement improved in images. In general, the workflow of AM is more intuitive and much more practical during
459 experimental stage. However, final results in terms of geolocalisation of the models and its geometrical qualities are in
460 favour of CC. In Table 2 we provide a more detailed qualitative comparison between the two tools.

Feature	Agisoft Metashape	ContextCapture
Performance economy	slower for all processes	faster for all processes (about 25%)
Geolocalisation procedure/ time involvement	can be done at any stage, mistakes can be mitigated at any step, overall the process is faster	can be done only before starting the SFM pipeline, mistakes can be mitigated only by repeating the procedure of calibration and all calculations, overall the process is slower
Minimum number of GCP	3 (for accuracy calculation 4)	3
Minimum number of scale-bars (for producing a model with correct scale)	2 (for accuracy calculation 3)	1 (for accuracy calculation 2)
Texture quality	good (on occasion, changing light during photography series is visible as a lighter coloured area on the model)	very good (better colour presentation, better colour blend, no lighter spots)
Texture options	Size, quality, colour blend, user chosen pictures for textures	Size of texture, user chosen pictures for textures
Reconstruction of fine details	Good (5 options) – oversmooths edges	Good (3 options) – better reconstruction of small details and preserves discontinuities in surface gradient
Option to manually remove artefacts within software	Yes	No
Depth reconstruction of concave areas, cracks, caves etc	Concavities visible only to an extent, mostly partly filled with mesh interpolation without meaningful depth	Concavities well reconstructed, no interpolated false depths
Artefacts, reconstruction of false elements	Large number on top and bottom of the models including models of clouds, distant mountain tops and glacier reflection in the water	Small number usually small random elements on top of the model

Mesh reconstruction options	Interpolation, extrapolation, none	None
Mesh voids	In all options (besides none) no voids in the mesh – software forces void filling	Voids occur where point cloud is too sparse

Tab. 2. Comparison of Agisoft Metashape and ContextCapture software performance – summary.

We demonstrate that this method is indeed effective for documentation of small-scale glacier dynamics, ContextCapture offers around 17% lower error, 25% faster processing and better reconstruction of fine details and shadowed concavities.

The accuracy we obtain in our Hans Glacier reconstructions can be compared to the similar experiment performed on much larger Russell Glacier, western Greenland [64], where time-lapse photography was used for SfM. The accuracy that was obtained in our experiment is the same order of magnitude as [64]; however, we are measuring a dynamic object with smaller daily front movement and in smaller time step. This forces us to find a means of creating more accurate models with smaller maximal to minimal error difference; this is provided by CC that also demonstrated 17% lower error than AM. Both experiments suggest that we are achieving close to the practical maximum performance of SfM, even in a challenging scenario. This accuracy may not be still as good as during terrestrial laser scanning [34] but provides sufficient spatial data for daily monitoring of glacier front changes in a scenario where laser scanning is impractical.

References

[1] M. Westoby, J. Brasington, N. Glasser, M. Hambrey, J. Reynolds, 'Structure-from-Motion' photogrammetry: A low-cost, effective tool for geoscience applications, Geomorphology. 179 (2012) 300–314. https://doi.org/10.1016/j.geomorph.2012.08.021.

[2] M.R. James, S. Robson, Straightforward reconstruction of 3D surfaces and topography with a camera: Accuracy and geoscience application, J. Geophys. Res. Earth Surf. 117 (2012) 1–17. https://doi.org/10.1029/2011JF002289.

[3] K. Anderson, M.J. Westoby, M.R. James, Low-budget topographic surveying comes of age: Structure from motion photogrammetry in geography and the geosciences, Prog. Phys. Geogr. 43 (2019) 163–173. https://doi.org/10.1177/0309133319837454.

[4] D.J.Q. Jonathan L. Carrivick, Mark W. Smith, Structure from Motion in the Geosciences, Wiley-Blackwell, 2016.

[5] M. Jaud, P. Letortu, C. Théry, P. Grandjean, S. Costa, O. Maquaire, R. Davidson, N. Le Dantec, UAV survey of a coastal cliff face – Selection of the best imaging angle, Meas. J. Int. Meas. Confed. 139 (2019) 10–20. https://doi.org/10.1016/j.measurement.2019.02.024.

[6] M. Rusnák, J. Sládek, A. Kidová, M. Lehotský, Template for high-resolution river landscape mapping using UAV technology, Meas. J. Int. Meas. Confed. 115 (2018) 139–151.

https://doi.org/10.1016/j.measurement.2017.10.023.

[7] W. Gruszczyński, W. Matwij, P. Ćwiąkakała, Comparison of low-altitude UAV photogrammetry with terrestrial laser scanning as data-source methods for terrain covered in low vegetation, ISPRS J. Photogramm. Remote Sens. 126 (2017) 168–179. https://doi.org/10.1016/j.isprsjprs.2017.02.015.

[8] B. Kršák, P. Blišťan, A. Pauliková, P. Puškárová, L. Kovanič, J. Palková, V. Zelizňaková, Use of low-cost UAV photogrammetry to analyze the accuracy of a digital elevation model in a case study, Meas. J. Int. Meas. Confed. 91 (2016) 276–287. https://doi.org/10.1016/j.measurement.2016.05.028.

[9] M. Zeybek, İ. Şanlıoğlu, Point cloud filtering on UAV based point cloud, Meas. J. Int. Meas. Confed. 133 (2019) 99–111. https://doi.org/10.1016/j.measurement.2018.10.013.

[10] H.-G. Maas, G. Casassa, D. Schneider, E. Schwalbe, A. Wendt, Photogrammetric determination of spatio-temporal velocity fields at Glaciar San Rafael in the Northern Patagonian Icefield, Cryosph. Discuss. 4 (2010) 2415–2432. https://doi.org/10.5194/tcd-4-2415-2010.

[11] P. Lewińska, D. Sowiński, S. Szombara, The measurements of snow cover volume in the area of Szrenicki Cirque, in: E3S Web Conf., 2018. https://doi.org/10.1051/e3sconf/20184900067.

[12] S. Harwin, A. Lucieer, Assessing the accuracy of georeferenced point clouds produced via multi-view stereopsis from Unmanned Aerial Vehicle (UAV) imagery, Remote Sens. 4 (2012) 1573–1599. https://doi.org/10.3390/rs4061573.

[13] M. Scaioni, M. Corti, G. Diolaiuti, D. Fugazza, M. Cernuschi, Local and general monitoring of Forni Glacier (Italian Alps) using multi-platform structure-from-motion photogrammetry, ISPRS - Int. Arch. Photogramm. Remote Sens. Spat. Inf. Sci. XLII-2/W7 (2017) 1547–1554. https://doi.org/10.5194/isprs-archives-XLII-2-W7-1547-2017.

[14] N. Mölg, T. Bolch, Structure-from-motion using historical aerial images to analyse changes in glacier surface elevation, Remote Sens. 9 (2017). https://doi.org/10.3390/rs9101021.

[15] V.K. Mali, S.N. Kuiry, Assessing the accuracy of high-resolution topographic data generated using freely available packages based on SfM-MVS approach, Meas. J. Int. Meas. Confed. 124 (2018) 338–350. https://doi.org/10.1016/j.measurement.2018.04.043.

[16] F. Agüera-Vega, F. Carvajal-Ramírez, P. Martínez-Carricondo, Assessment of photogrammetric mapping accuracy based on variation ground control points number using unmanned aerial vehicle, Meas. J. Int. Meas. Confed. 98 (2017) 221–227. https://doi.org/10.1016/j.measurement.2016.12.002.

[17] Agisoft Metashape, (n.d.). https://www.agisoft.com/ (accessed May 13, 2020).

[18] ContexCapture Bentley, (n.d.). https://www.bentley.com/en/products/product-line/reality-modeling-software/contextcapture (accessed May 13, 2020).

[19] A.S. Gardner, G. Moholdt, J.G. Cogley, B. Wouters, A.A. Arendt, J. Wahr, E. Berthier, R. Hock, W.T. Pfeffer, G. Kaser, S.R.M. Ligtenberg, T. Bolch, M.J. Sharp, J.O. Hagen, M.R. van den Broeke, F. Paul, A Reconciled Estimate of Glacier Contributions to Sea Level Rise: 2003 to 2009, Science (80-.). 340 (2013) 852–857. https://doi.org/10.1126/science.1234532.

[20] J. Bamber, M. Van Den Broeke, J. Ettema, J. Lenaerts, E. Rignot, Recent large increases in freshwater fluxes from Greenland into the North Atlantic, Geophys. Res. Lett. 39 (2012) 8–11. https://doi.org/10.1029/2012GL052552.

[21] E.J. Rahmstorf, Stefan ; Box, Jason E. ; Feulner, Georg ; Mann, Michael E. ; Robinson, Alexander ; Rutherford, Scott ; Schaffernicht, Exceptional twentieth-century slowdown in Atlantic Ocean overturning circulation., Nat. Clim. Chang. 5 (2015) 475–480. https://doi.org/10.1038/nclimate2554.

[22] R.J. Motyka, L. Hunter, K.A. Echelmeyer, C. Connor, Submarine melting at the terminus of a temperate tidewater glacier, LeConte Glacier, Alaska, U.S.A., Ann. Glaciol. 36 (2003) 57–65. https://doi.org/10.3189/172756403781816374.

[23] V.B. and P.M.M. Stocker, T.F., D. Qin, G.-K. Plattner, M. Tignor, S.K. Allen, J. Boschung, A. Nauels, Y. Xia, IPCC, 2013: Climate Change 2013: The Physical Science Basis. Contribution of Working Group I to the Fifth Assessment Report of the Intergovernmental Panel on Climate Change, Cambridge, United Kingdom and New York, NY, USA, 2018.

[24] D.I. Benn, C.R. Warren, R.H. Mottram, Calving processes and the dynamics of calving glaciers, Earth-Science Rev. 82 (2007) 143–179. https://doi.org/10.1016/j.earscirev.2007.02.002.

[25] E.M. Enderlin, I.M. Howat, S. Jeong, M.-J. Noh, J.H. van Angelen, M.R. van den Broeke, An improved mass budget for the Greenland ice sheet, Geophys. Res. Lett. 41 (2014) 866–872. https://doi.org/10.1002/2013GL059010.

[26] M.R. Van Den Broeke, E.M. Enderlin, I.M. Howat, P. Kuipers Munneke, B.P.Y. Noël, W. Jan Van De Berg, E. Van Meijgaard, B. Wouters, On the recent contribution of the Greenland ice sheet to sea level change, Cryosphere. 10 (2016) 1933–1946. https://doi.org/10.5194/tc-10-1933-2016.

[27] M. Błaszczyk, J.A. Jania, J.O. Hagen, Tidewater glaciers of Svalbard: Recent changes and estimates of calving fluxes, Polish Polar Res. 30 (2009) 85–142.

[28] D. Mansell, A. Luckman, T. Murray, Dynamics of tidewater surge-type glaciers in northwest Svalbard, J. Glaciol. 58 (2012) 110–118. https://doi.org/10.3189/2012JoG11J058.

[29] W.W. Immerzeel, P.D.A. Kraaijenbrink, J.M. Shea, A.B. Shrestha, F. Pellicciotti, M.F.P. Bierkens, S.M. [de Jong], High-resolution monitoring of Himalayan glacier dynamics using unmanned aerial vehicles, Remote Sens. Environ. 150 (2014) 93–103. https://doi.org/https://doi.org/10.1016/j.rse.2014.04.025.

[30] T.R. Chudley, P. Christoffersen, S.H. Doyle, A. Abellan, N. Snooke, High-accuracy UAV photogrammetry of ice sheet dynamics with no ground control, Cryosphere. 13 (2019) 955–968. https://doi.org/10.5194/tc-13-955-2019.

[31] T. Murray, N. Selmes, T.D. James, S. Edwards, I. Martin, T. O'Farrell, R. Aspey, I. Rutt, M. Nettles, T. Baugé, Dynamics of glacier calving at the ungrounded margin of Helheim Glacier, southeast Greenland., J. Geophys. Res. Earth Surf. 120 (2015) 964–982. https://doi.org/10.1002/2015JF003531.

[32] D. Vallot, S. Adinugroho, R. Strand, P. How, R. Pettersson, D.I. Benn, N.R.J. Hulton, Automatic detection of calving events from time-lapse imagery at Tunabreen, Svalbard, Geosci. Instrumentation, Methods Data Syst. 8 (2019) 113–127. https://doi.org/10.5194/gi-8-113-2019.

[33] A. Chapuis, C. Rolstad, R. Norland, Interpretation of amplitude data from a ground-based radar in combination with terrestrial photogrammetry and visual observations for calving monitoring of Kronebreen, Svalbard, Ann. Glaciol. 51 (2010) 34–40. https://doi.org/10.3189/172756410791392781.

[34] M. Pętlicki, C. Kinnard, Calving of Fuerza Aérea Glacier (Greenwich Island, Antarctica) observed with terrestrial laser scanning and continuous video monitoring, J. Glaciol. 62 (2016) 835–846. https://doi.org/10.1017/jog.2016.72.

[35] P.J. Gadomski, D.C. Finnegan, A.L. LeWinter, L.A. Stearns, C.M. Kershner, G. Hanlon, Three summer of high-resolution, high-accuracy velocity data of Helheim Glacier, as measured by an automated terrestrial LiDAR scanner: methods, challenges, and applications, AGU Fall Meet. Abstr. (2017) 6–7. https://doi.org/10.13140/RG.2.2.24369.07528.

[36] D.C. Finnegan, G.S. Hamilton, A. LeWinter, P.J. Gadomski, L.A. Stearns, C.M. Kershner, High-Resolution Tidewater Glacier Monitoring Using Automated Multi-Temporal Terrestrial LiDAR; Year One Results, Helheim Glacier, Southeast Greenland, in: AGU Fall Meet. Abstr., 2016: pp. C41C-0687.

[37] D.C. Finnegan, A. LeWinter, G.S. Hamilton, P.J. Gadomski, L.A. Stearns, Long-term Autonomous Tidewater Glacier Monitoring Using a Long-Range Terrestrial LiDAR Scanner; Helheim Glacier, Southeast Greenland, in: AGU Fall Meet. Abstr., 2015: pp. C43B-0807.

[38] A.L. LeWinter, D.C. Finnegan, G.S. Hamilton, L.A. Stearns, P.J. Gadomski, Continuous Monitoring of Greenland Outlet Glaciers Using an Autonomous Terrestrial LiDAR Scanning System: Design, Development and Testing at Helheim Glacier, in: AGU Fall Meet. Abstr., 2014: pp. C31B-0292.

[39] A. Wójcik, P. Klapa, B. Mitka, I. Piech, The use of TLS and UAV methods for measurement of the repose angle of granular materials in terrain conditions, Meas. J. Int. Meas. Confed. 146 (2019) 780–791. https://doi.org/10.1016/j.measurement.2019.07.015.

[40] C. Rohner, D. Small, D. Henke, M.P. Lüthi, A. Vieli, Multisensor validation of tidewater glacier flow fields derived from synthetic aperture radar (SAR) intensity tracking, Cryosphere. 13 (2019) 2953–2975. https://doi.org/10.5194/tc-13-2953-2019.

[41] D.M. Holland, D. Voytenko, K. Christianson, T.H. Dixon, M.J. Mei, B.R. Parizek, I. Vaňková, R.T. Walker, J.I. Walter, K. Nicholls, D. Holland, An intensive observation of calving at Helheim Glacier, East Greenland, Oceanography. 29 (2016) 46–61. https://doi.org/10.5670/oceanog.2016.98.

[42] L. Piermattei, L. Carturan, A. Guarnieri, Use of terrestrial photogrammetry based on structure-from-motion for mass balance estimation of a small glacier in the Italian alps, Earth Surf. Process. Landforms. 40 (2015) 1791–1802. https://doi.org/10.1002/esp.3756.

[43] J.C. Ely, C. Graham, I.D. Barr, B.R. Rea, M. Spagnolo, J. Evans, Using UAV acquired photography and structure from motion techniques for studying glacier landforms: application to the glacial flutes at Isfallsglaciären, Earth Surf. Process. Landforms. 42 (2017) 877–888. https://doi.org/10.1002/esp.4044.

[44] L. Benoit, A. Gourdon, R. Vallat, I. Irarrazaval, M. Gravey, G. Prasicek, D. Gräff, F. Herman, G. Mariethoz, Gornergletscher - Swiss Alps - derived from repeated UAV surveys, Earth Syst. Sci. Data. 30 (2018) 1–17.

[45] L. Piermattei, L. Carturan, F. De Blasi, P. Tarolli, G. Dalla Fontana, A. Vettore, N. Pfeifer, Suitability of ground-based SfM-MVS for monitoring glacial and periglacial processes, Earth Surf. Dyn. 4 (2016) 425–443. https://doi.org/10.5194/esurf-4-425-2016.

[46] Roze, A., Zufferey, J.C., Beyeler, A., McClellan, A., eBee RTK Accuracy Assessment, White Paper, SenseFly. (2014).

[47] N.G. Midgley, T.N. Tonkin, Reconstruction of former glacier surface topography from archive oblique aerial images, Geomorphology. 282 (2017) 18–26. https://doi.org/10.1016/j.geomorph.2017.01.008.

[48] M.R. James, S. Robson, Mitigating systematic error in topographic models derived from UAV and ground-based image networks, Earth Surf. Process. Landforms. 39 (2014) 1413–1420. https://doi.org/10.1002/esp.3609.

[49] J.C. Ryan, A.L. Hubbard, J.E. Box, J. Todd, P. Christoffersen, J.R. Carr, T.O. Holt, N. Snooke, UAV photogrammetry and structure from motion to assess calving dynamics at Store Glacier, a large outlet draining the Greenland ice sheet, Cryosphere. 9 (2015) 1–11. https://doi.org/10.5194/tc-9-1-2015.

[50] H. Yurtseven, M. Akgul, S. Coban, S. Gulci, Determination and accuracy analysis of individual tree crown parameters using UAV based imagery and OBIA techniques, Meas. J. Int. Meas. Confed. 145 (2019) 651–664.

https://doi.org/10.1016/j.measurement.2019.05.092.

[51] H. Park, D. Lee, Comparison between point cloud and mesh models using images from an unmanned aerial vehicle, Meas. J. Int. Meas. Confed. 138 (2019) 461–466. https://doi.org/10.1016/j.measurement.2019.02.023.

[52] J. Liénard, A. Vogs, D. Gatziolis, N. Strigul, Embedded, real-time UAV control for improved, image-based 3D scene reconstruction, Meas. J. Int. Meas. Confed. 81 (2016) 264–269. https://doi.org/10.1016/j.measurement.2015.12.014.

[53] X.S. Gao, X.R. Hou, J. Tang, H.F. Cheng, Complete solution classification for the perspective-three-point problem, IEEE Trans. Pattern Anal. Mach. Intell. 25 (2003) 930–943. https://doi.org/10.1109/TPAMI.2003.1217599.

[54] R.A.Z. Hartley;, Multiple View Geometry in Computer Vision Second Edition, Cambridge University Press, 2003.

[55] D.G. Lowe, Distinctive Image Features from Scale-Invariant Keypoints, Int. J. Comput. Vis. 60 (2004) 91–110. https://doi.org/10.1023/B:VISI.0000029664.99615.94.

[56] K. Maciuk, The study of seasonal changes of permanent stations coordinates based on weekly EPN solutions, Artif. Satell. J. Planet. Geod. 51 (2016) 1–18. https://doi.org/10.1515/arsa-2016-0001.

[57] C. Strecha, R. Fransens, L. Van Gool, Combined Depth and Outlier Estimation in Multi-View Stereo, in: 2006 IEEE Comput. Soc. Conf. Comput. Vis. Pattern Recognit., 2006: pp. 2394–2401. https://doi.org/10.1109/CVPR.2006.78.

[58] I. Shim, T.H. Oh, I.S. Kweon, High-fidelity depth upsampling using the self-learning framework, Sensors (Switzerland). 19 (2019) 1–18. https://doi.org/10.3390/s19010081.

[59] C. Veen, Calving glaciers, Prog. Phys. Geogr. - PROG PHYS GEOG. 26 (2002) 96–122. https://doi.org/10.1191/0309133302pp327ra.

[60] P. How, K.M. Schild, D.I. Benn, R. Noormets, N. Kirchner, A. Luckman, D. Vallot, N.R.J. Hulton, C. Borstad, Calving controlled by melt-under-cutting: detailed calving styles revealed through time-lapse observations, Ann. Glaciol. 60 (2019) 20–31. https://doi.org/10.1017/aog.2018.28.

[61] T.D. James, T. Murray, N. Selmes, K. Scharrer, M. O'Leary, Buoyant flexure and basal crevassing in dynamic mass loss at Helheim Glacier, Nat. Geosci. 7 (2014) 593–596. https://doi.org/10.1038/ngeo2204.

[62] M. Minowa, E.A. Podolskiy, S. Sugiyama, D. Sakakibara, P. Skvarca, Glacier calving observed with time-lapse imagery and tsunami waves at Glaciar Perito Moreno, Patagonia, J. Glaciol. 64 (2018) 362–376. https://doi.org/10.1017/jog.2018.28.

[63] A. Köhler, M. Pętlicki, P.-M. Lefeuvre, G. Buscaino, C. Nuth, C. Weidle, Contribution of calving to frontal ablation quantified from seismic and hydroacoustic observations calibrated with lidar volume measurements, Cryosph. 13 (2019) 3117–3137. https://doi.org/10.5194/tc-13-3117-2019.

[64] J. Mallalieu, J.L. Carrivick, D.J. Quincey, M.W. Smith, W.H.M. James, An integrated Structure-from-Motion and time-lapse technique for quantifying ice-margin dynamics, J. Glaciol. 63 (2017) 937–949. https://doi.org/10.1017/jog.2017.48.

[65] C. Nuth, J. Kohler, M. König, A. Von Deschwanden, J.O. Hagen, A. Kääb, G. Moholdt, R. Pettersson, Decadal changes from a multi-temporal glacier inventory of Svalbard, Cryosphere. 7 (2013) 1603–1621. https://doi.org/10.5194/tc-7-1603-2013.

[66] A.A. Bjørk, K.H. Kjær, N.J. Korsgaard, S.A. Khan, K.K. Kjeldsen, C.S. Andresen, J.E. Box, N.K. Larsen, S. Funder, An aerial view of 80 years of climate-related glacier fluctuations in southeast Greenland, Nat. Geosci. 5 (2012) 427–432. https://doi.org/10.1038/ngeo1481.

[67] K.H. Kjær, S.A. Khan, N.J. Korsgaard, J. Wahr, J.L. Bamber, R. Hurkmans, M. van den Broeke, L.H. Timm, K.K. Kjeldsen, A.A. Bjørk, N.K. Larsen, L.T. Jørgensen, A. Færch-Jensen, E. Willerslev, Aerial Photographs Reveal Late–20th-Century Dynamic Ice Loss in Northwestern Greenland, Science (80-.). 337 (2012) 569 LP – 573. https://doi.org/10.1126/science.1220614.

[68] N.S. Arnold, W.G. Rees, B.J. Devereux, G.S. Amable, Evaluating the potential of high-resolution airborne LiDAR data in glaciology, Int. J. Remote Sens. 27 (2006) 1233–1251. https://doi.org/10.1080/01431160500353817.

[69] C.S. Watson, D.J. Quincey, M.W. Smith, Jo.L. Carrivck, A.N.N. V Rowan, M.R. James, Quantifying ice cliff evolution with multi-temporal point clouds on the debris-covered Khumbu Glacier, Nepal, J. Glaciol. 63 (2017) 823–837. https://doi.org/10.1017/jog.2017.47.

[70] M. Stober, J. Hepperle, Changes in ice elevation and ice flow-velocity in the Swiss Camp area (West Greenland) between 1991 and 2006, Polarforschung. 76 (2006) 109–118.

[71] R. Rosenau, E. Schwalbe, H.-G. Maas, M. Baessler, R. Dietrich, Grounding line migration and high-resolution calving dynamics of Jakobshavn Isbræ, West Greenland, J. Geophys. Res. Earth Surf. 118 (2013) 382–395. https://doi.org/10.1029/2012JF002515.

[72] M.R. James, P. How, P.M. Wynn, Pointcatcher software: analysis of glacial time-lapse photography and integration with multitemporal digital elevation models, J. Glaciol. 62 (2016) 159–169. https://doi.org/10.1017/jog.2016.27.

[73] T. Bradwell, O. Sigurdsson, J. Everest, Recent, very rapid retreat of a temperate glacier in SE Iceland, Boreas.

673 42 (2013) 959–973. https://doi.org/10.1111/bor.12014.

674 [74] M. Tomkins, Tracking retreat processes at the Falljökull Glacier, SE Iceland, Lancaster University, 2016.

675 [75] D. Medrzycka, D.I. Benn, J.E. Box, L. Copland, J. Balog, Calving Behavior at Rink Isbræ, West Greenland,
676 from Time-Lapse Photos, Arctic, Antarct. Alp. Res. 48 (2016) 263–277. https://doi.org/10.1657/AAAR0015-
677 059.

678 [76] K.M. Schild, R.L. Hawley, B.F. Morriss, Subglacial hydrology at Rink Isbræ, West Greenland inferred from
679 sediment plume appearance, Ann. Glaciol. 57 (2016) 118–127. https://doi.org/10.1017/aog.2016.1.

680 [77] F.J. Navarro, A. Martín-Español, J.J. Lapazaran, M. Grabiec, J. Otero, E. V Vasilenko, D. Puczko, Ice Volume
681 Estimates from Ground-Penetrating Radar Surveys, Wedel Jarlsberg Land Glaciers, Svalbard, Arctic, Antarct.
682 Alp. Res. 46 (2014) 394–406. https://doi.org/10.1657/1938-4246-46.2.394.

683 [78] O. Glowacki, G.B. Deane, M. Moskalik, P. Blondel, J. Tegowski, M. Blaszczyk, Underwater acoustic
684 signatures of glacier calving, Geophys. Res. Lett. 42 (2015) 804–812. https://doi.org/10.1002/2014GL062859.

685 [79] Cloud Compare, (n.d.). https://www.danielgm.net/cc/ (accessed May 13, 2020).

686 [80] T. Moon, I. Joughin, B. Smith, I. Howat, 21st-Century Evolution of Greenland Outlet Glacier Velocities,
687 Science (80-.). 336 (2012) 576–578. https://doi.org/10.1126/science.1219985.

688 [81] M. Błaszczyk, D. Ignatiuk, A. Uszczyk, K. Cielecka-Nowak, M. Grabiec, J.A. Jania, M. Moskalik, W.
689 Walczowski, Freshwater input to the arctic fjord hornsund (Svalbard), Polar Res. 38 (2019) 1–18.
690 https://doi.org/10.33265/polar.v38.3506.

691